

Photoionization and electron–ion recombination of P II

Sultana N. Nahar[★]

Department of Astronomy, Ohio State University, Columbus, OH 43210, USA

Accepted 2017 April 18. Received 2017 April 16; in original form 2016 July 7

ABSTRACT

A study of the inverse processes of photoionization and electron–ion recombination of P II is reported. Phosphorus, a little studied cosmic element, requires atomic parameters such as those presented here for spectral analysis. The unified method of Nahar and Pradhan, which incorporates two methods of recombination – radiative recombination (RR) and dielectronic recombination (DR) – and the interference between them, is used to obtain the total electron–ion recombination. This method implements the framework of the **R**-matrix close-coupling approximation. The present results include the partial photoionization cross-sections $\sigma_{PI}(J\pi)$ leaving the residual ion in the ground level and level-specific recombination rate coefficients, $\alpha_{RC}(J\pi)$, of 475 fine-structure levels of P II with $n \leq 10$. In photoionization of the ground and many excited levels, a sharp resonance is found to form at the ionization threshold from couplings of relativistic fine-structure channels. These, with other resonances in the near-threshold energy region, yield a slight curvature, in contrast to typical smooth decay, at a very low temperature of about 330 K in the total recombination rate coefficient α_{RC} . The presence of other Rydberg and Seaton resonances in the photoionization cross-section introduces features in the level-specific recombination rate coefficients and a DR bump at high temperature at 10^5 K for the total recombination rate coefficient. Considerable interference between RR and DR is noted around 6700 K. The recombination spectrum with respect to photoelectron energy $\alpha_{RC}(E)$ is also presented. The results are expected to provide accurate models for astrophysical plasmas up to ~ 1 MK.

Key words: atomic data – atomic processes – line formation – stars: abundances – galaxies: abundances.

1 INTRODUCTION

Phosphorus is a primary element in the ribonucleic acid (RNA) of all living cells and functions in signal passing for DNA. However, its detection has been difficult in comparison with other basic elements of life, such as carbon, oxygen, etc. Recently, it has been detected in a number of astronomical objects, e.g. in damp galaxies by Molaro et al. (2001) and Welsh et al. (2001). Lines of P II and P III have been found in the high-resolution spectra of hot OB stars under a project called ASTRO-2 (J. Hillier, private communication).

It is a highly reactive ion and there is a lack of detailed information regarding its atomic interactions, which is needed for spectral analysis. P II is a Si-like ion, but due to its low abundance it was not studied under the Opacity Project (Seaton 1987; Opacity Project Team (OP) 1995, 1996) until recently by Nahar (2017) and Nahar et al. (2017). The photoionization cross-section of P II at low energy was measured with high precision at the Advanced Light Source (ALS) by Hinojosa et al. (2015). The features have been studied in

detail and were identified theoretically using the **R**-matrix method (Nahar et al. 2017).

The present work focuses on photoionization and electron–ion recombination processes, which are inverse to each other, as expressed below:

$$h\nu + X^+ \leftrightarrow e + X^{++}, \quad (1)$$

where X^+ is an ion. The above equation expresses direct photoionization and electron–ion recombination, where the latter is called radiative recombination (RR) and appears as featureless background cross-sections. However, when the energy matches a level of the Rydberg series $(S;L_iJ_i\pi_i)\nu l$ above the ionization energy, an intermediate doubly excited autoionizing state is formed. $(S;L_iJ_i\pi_i)$ is an excited level of the core and νl , where ν is the effective quantum number, which is the quantum level of the outer excited electron of the ion such that the Rydberg series of levels converges on to the excited core. The autoionizing state is a quasi-bound state and breaks down to either autoionization (AI), where the interacting electron goes into the continuum, or dielectronic recombination (DR), where it is captured by emission of a photon (e.g. Pradhan & Nahar 2011):

$$e + X^{++} \leftrightarrow (X^+)^{**} \leftrightarrow \begin{cases} \text{(a) } e + X^{++}(\text{AI}), \\ \text{(b) } h\nu + X^+(\text{DR}). \end{cases} \quad (2)$$

[★] E-mail: nahar.1@osu.edu

An autoionizing state is manifested as a resonance in the process. A resonance can be calculated naturally by including the core excitation in the wavefunction, such as is considered in the close coupling (CC) approximation used in the present work.

The present work reports features of partial cross-sections, in contrast to earlier total (Nahar 2016) photoionization, leaving the core in the ground level. Although similar, it is a separate computation from the earlier one. These cross-sections are needed to obtain the recombination cross-sections and rates for P II.

2 THEORY

The unified method for the total electron–ion recombination (Nahar & Pradhan 1992, 1994; Zhang, Nahar & Pradhan 1999; Pradhan & Nahar 2011) considers the unified nature of the (e + ion) recombination process by including both the RR and DR and their interference. Hence it gives the total recombination rate. The method implements the framework of the close-coupling approximation (CC) and **R**-matrix method and provides a self-consistent set of atomic parameters for photoionization and electron–ion recombination. The relativistic effects are included in the Breit–Pauli **R**-matrix (BPRM) method as developed under the Iron Project (Hummer et al. 1993; Pradhan & Nahar 2011).

In the CC approximation, the total wavefunction $\Psi(E)$ is expressed as an expansion of wavefunctions χ_i of the core of N electrons multiplied by the interacting ($N+1$)th electron wavefunction θ :

$$\Psi(E) = A \sum_i \chi_i \theta_i + \sum_j c_j \Phi_j. \quad (3)$$

The sum in the first term is over the number of the ground and various excited states of the residual or core ion. The second term, basically part of the first term, contains the bound-channel functions Φ_j of the ($N+1$)-electron system to account for short-range correlation and the orthogonality between the continuum and the bound orbitals. Substitution of the expansion in the Schrodinger equation results in a set of coupled equations, which is solved for energies and wavefunctions using the **R**-matrix method. The wavefunction $\Psi(E)$ of channel $S_i L_i (J_i) \pi_i k_i^2 \ell_i$ ($SL\pi$ or $J\pi$), where k_i^2 is the kinetic energy of the interacting electron, corresponds to a bound state Ψ_B for $E < 0$ or a continuum state Ψ_F for $E > 0$. Interference of the bound and continuum channels with the excited core in the transition matrix introduces resonances.

The transition matrix element $\langle \Psi_B || \mathbf{D} || \Psi_F \rangle$, where $\mathbf{D} = \sum_i r_i$ is the dipole operator and the sum is over the number of electrons, gives the line strength as

$$S = |\langle \Psi_B || \mathbf{D} || \Psi_F \rangle|^2. \quad (4)$$

The photoionization cross-section, σ_{PI} , is obtained from the line strength as

$$\sigma_{\text{PI}} = \frac{4\pi^2}{3g_i c} \omega S, \quad (5)$$

where g_i is the statistical weight factor of the initial bound state. Assuming the recombining ion is in its ground state, σ_{PI} corresponds to a partial photoionization cross-section, leaving the ion in the ground state. The radiation damping effect of autoionizing resonances is included using a scheme developed by Sakimoto et al. (1990), Pradhan & Zhang (1997) and Zhang et al. (1999).

The unified method obtains the level-specific electron–ion recombination cross-section σ_{RC} for levels up to $n \leq n_o$, which is typically

10, from photoionization cross-sections σ_{PI} using the principle of detailed balance:

$$\sigma_{\text{RC}}(\epsilon) = \frac{\alpha^2 g_i (\epsilon + I)^2}{4 g_j \epsilon} \sigma_{\text{PI}}. \quad (6)$$

The equation is expressed in atomic units. ϵ is the photoelectron energy in Ry, g_j is the statistical weight factor of the recombined ion, I is the ionization potential and α is the fine-structure constant. The total recombination cross-section, σ_{RC} , is the summed contribution of all recombined levels. This sum also gives the location and strength of diagnostic dielectronic satellite (DES) lines of the ion in hot plasmas. However, the DES lines are identifiable only for a few electron systems where overlapping of resonances is small.

The unified method includes contributions of states with $n_o < n \leq \infty$, which are closely lying narrow resonances and are dominated by DR, through the quantum-defect theory of DR within the close-coupling approximation (Bell & Seaton 1985; Nahar & Pradhan 1994). They are obtained in the form of recombination collision strength, Ω_{RC} , which is related to the recombination cross-section, σ_{RC} in Mb, by

$$\sigma_{\text{RC}}(i \rightarrow j)(\text{Mb}) = \frac{\pi}{g_i k_i^2} \Omega_{\text{RC}}(i, j) (\alpha_o^2 / 10^{-18}), \quad (7)$$

where k_i^2 is the electron energy in Ry. Ω_{RC} is a numerically stable quantity compared with σ_{RC} , which diverges at zero photoelectron energy. The non-resonant background contribution of these states, referred to as the ‘high- n top-up’, is added in the hydrogenic approximation (Nahar 1996). This contribution is negligible except at very low temperature, where DR may not be accessible by a low-energy electron.

The recombination rate coefficient, $\alpha_{\text{R}}(nSLJ)$, of a recombined level $i = nSLJ$ at temperature T is obtained by averaging the recombination cross-sections $\sigma_{\text{RC}}(i)$ over a Maxwellian electron distribution function $f(v, T)$ as

$$\alpha_{\text{R}}(i, T) = \int_0^\infty v f(v, T) \sigma_{\text{RC}}(i) dv, \quad (8)$$

where

$$f(v) = \frac{4}{\sqrt{\pi}} \left(\frac{m}{2kT} \right)^{3/2} v^2 e^{-(mv^2)/(2kT)}. \quad (9)$$

These individual rate coefficients $\sum_i \alpha_{\text{R}}(i, T)$ are summed for the total recombination rate coefficient, α_{R} .

The features of the recombination rate coefficients $\alpha_{\text{RC}}(E)$ with respect to photoelectron energy E are of interest, as these can be measured experimentally (e.g. Pradhan, Nahar & Zhang 2001). $\alpha_{\text{RC}}(E)$ with photoelectron velocity v can be obtained as

$$\alpha_{\text{RC}}(E) = v \sigma_{\text{RC}}(E). \quad (10)$$

The observed recombination spectra of $\alpha_{\text{RC}}(E)$ are typically convolved with the monochromatic bandwidth of the experimental beam in synchrotron facilities such as the Test Storage Ring in Heidelberg.

3 COMPUTATIONS

The calculation for the partial photoionization cross-sections was carried out using the Breit–Pauli **R**-matrix (BPRM) package of codes (Berrington, Eissner & Norrington 1995; Nahar & Pradhan 1994; Zhang et al. 1999). These codes were extended extensively from the original codes (Burke & Taylor 1975; Scott & Burke 1980). The energies of the 18 levels of the core ion P III used in the

Table 1. Energies (E_i) of core (P III) levels included in the wavefunction expansion of P II. Calculated energies are compared with those from the NIST tabulations (http://physics.nist.gov/PhysRefData/ASD/levels_form.html). The last column (E1) gives the radiative decay rates (A values) for dipole allowed transitions to the ground level.

Level	J_i	E_i (Ry) NIST	E_i (Ry) SS	A_{ji} (s^{-1}) E1 ($j - 1$)
1	3s ² 3p(² P ^o)	1/2	0.0	0.
2	3s ² 3p(² P ^o)	3/2	0.005095	0.00429
3	3s3p(⁴ P)	5/2	0.523559	0.51278
4	3s3p(⁴ P)	3/2	0.520570	0.51028
5	3s3p(⁴ P)	1/2	0.518708	0.50874
6	3s3p(² D)	3/2	0.682693	0.70551
7	3s3p(² D)	5/2	0.682957	0.70565
8	3s3p(² S)	1/2	0.913094	0.99414
9	3s3p(² P)	1/2	0.993621	1.03335
10	3s3p(² P)	3/2	0.997044	1.03613
11	3s ² 3d(² D)	3/2	1.065039	1.14381
12	3s ² 3d(² D)	5/2	1.065142	1.14392
13	3s ² 4s(² S)	1/2	1.073800	1.10909
14	3s ² 4p(² P ^o)	1/2	1.28832	1.34867
15	3s ² 4p(² P ^o)	3/2	1.28956	1.34955
16	3p ³ (² D ^o)	3/2	1.342508	1.38637
17	3p ³ (² D ^o)	5/2	1.343073	1.38678
18	3p ³ (⁴ S ^o)	3/2	1.455433	1.49071

close-coupling wavefunction expansion Ψ (equation 3) were obtained from the atomic structure calculations of 19 configurations using the code SUPERSTRUCTURE (SS: Eissner, Jones & Nussbaumer 1974; Nahar et al. 2003) and are listed in Table 1. They are the same as those used earlier by Nahar (2017). We note, that with an increased number of levels in the close-coupling expansion, more resonances are introduced and background cross-sections vary as the close-coupling expansion slowly converges. However, for the present energy range investigated, the above 18-level approximation provides an adequate representation, as illustrated in our recent theoretical/experimental investigation on this system (Nahar et al. 2017). It adequately reproduces the high-resolution ALS experimental measurements, as indicated in the recent work by Nahar et al. (2017).

The core ion wavefunctions χ_i of equation (3) for these levels are used as the initial input for the BPRM stages of computation. For improved accuracy of the energy positions of the resonances, calculated energies were replaced by the observed energies available in the energy table compiled at the National Institute of Standards and Technology website (NIST) (discussed in Nahar 2016). The second term of Ψ included 39 configurations of P II (Nahar 2016).

Table 1 gives the radiative decay rates or A values for dipole allowed (E1) transitions to the ground level. They were obtained using the program *ss*. These dipole allowed transitions introduce series of stronger autoionizing resonances at energy positions of Rydberg states $S_i L_i J_i \pi_i \nu l$ belonging to core state $S_i L_i J_i \pi_i$. They also introduce Seaton resonances caused by photo-excitation of the core (PEC: Yu & Seaton 1987) at the excited thresholds. These are discussed later.

The photoionization cross-section σ_{PI} beyond the resonant region can be extended to the high-energy region by extrapolation using the fitting formula

$$\sigma_{PI}(E) = aE^b, \quad (11)$$

where the values of parameters a and b are determined from two cross-sections σ_1 and σ_2 at energies E_1 and E_2 before the beginning

of extrapolation as

$$b = \log\left(\frac{\sigma_1}{\sigma_2}\right) / \log\left(\frac{E_1}{E_2}\right),$$

$$\log(a) = \{\log(\sigma_1) + \log(\sigma_2) - b[\log(E_1) + \log(E_2)]\} / 2.$$

The condition on parameter b is $0 > b \geq -3$. At energies where the condition is not satisfied and at very high energies, Kramer's fit

$$\sigma_{PI}(E) = \sigma_o \left(\frac{E_o}{E}\right)^3 \quad (12)$$

is used σ_o is the cross-section at energy E_o where the extrapolation begins.

The level-specific recombination rate coefficients $\alpha_R(i)$ of levels with $n \leq 10$ were obtained from the code RECXS (Nahar, Pradhan & Zhang 2000). The integration for $\alpha_{RC}(T)$ extends to ∞ in energy. For fast convergence, the rate-coefficient equation was converted to this form:

$$\alpha_{RC}(T) = -\frac{g_i}{g_j} \frac{2}{c^2 \sqrt{2\pi m^3 k T}} \int_1^0 [I - kT \log(x)]^2 \sigma_{PI} dx \quad (13)$$

in the high-energy region $x = \exp(-E/kT)$, which has slow variation at low and fast variation at high T . The sum of $\alpha_{RC}(i, T)$ gives the main contribution to the total. The DR collision strengths for the narrow and dense resonances in the energy region $10 < \nu \leq \infty$ below each target excited threshold were obtained using STGFDR (Nahar & Pradhan 1994; Zhang et al. 1999). The radiative decay rates needed for the \mathbf{S} -matrix evaluation are given in Table 1. The RR background contributions from all $n \leq \infty$ were added in the hydrogenic approximation, as described in Nahar (1996).

4 RESULTS AND DISCUSSION

The inverse processes of photoionization and electron-ion recombination of P II have been studied using the unified method of Nahar & Pradhan (1992, 1994). Various features of the two processes and their correspondences are discussed in two separate sections below.

4.1 Photoionization

The present work considers photoionization of P II leaving the core in its ground level 3s²3p(²P_{1/2}^o) and reports photoionization cross-sections (σ_{PI}) of 475 levels with $n \leq 10$. Elaborate features in σ_{PI} that contribute to electron-ion recombination for P II are illustrated with examples.

Fig. 1 shows σ_{PI} of (a) the ground and (b) and (c) two excited levels of P II that display certain characteristics in resonances over an energy region. Each level shows a resonance at the threshold. The resonance has been formed by relativistic effects, mainly the relativistic fine-structure channels 3s²3p(²P_{3/2}^o) νl , which do not exist in the LS coupling approximation (Nahar 2016). These resonances have been observed experimentally (Hinojosa et al. 2015; Nahar et al. 2017). The threshold resonance is found to exist in the photoionization cross-sections of many other excited levels. Fig. 1 also shows the extended energy region beyond the threshold featured by resonances. These resonances are the Rydberg series of resonances that belong to various excited levels of the core ion. The existence of these resonance complexes is common for low-lying excited levels when electron-electron interactions are strong for multi-electron systems. These low-energy resonant features of Fig. 1 can have an impact on quantities such as recombination rates, photoionization rates, etc., at low temperature. For the present case, these resonant features have introduced a slight curvature in the low-temperature

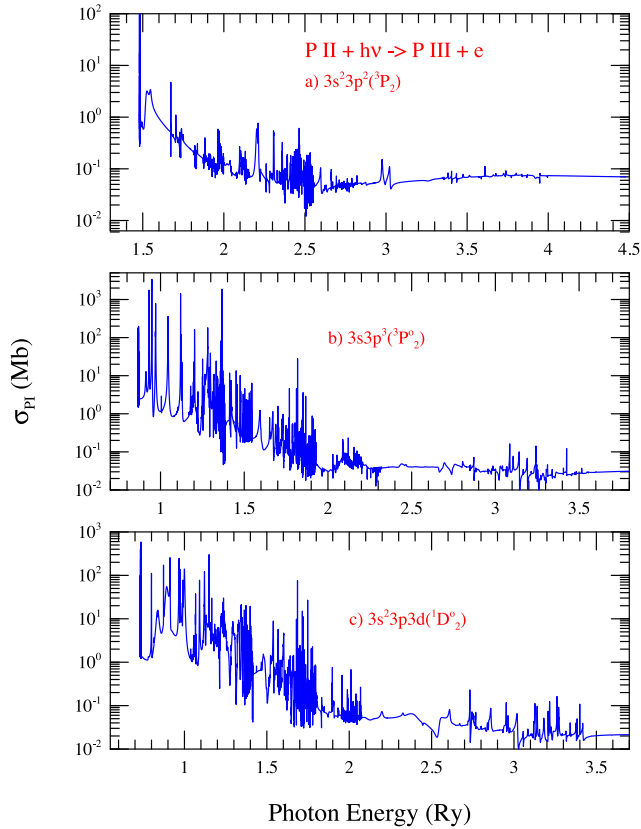


Figure 1. Photoionization cross-section σ_{PI} of (a) the ground $3s^2 3p^2 (3P_2)$ and two excited (b) $3s 3p^3 ({}^3P_2^o)$ and (c) $3s^2 3p 3d ({}^1D_2^o)$ levels of P II, showing the characteristic features of threshold resonance and an extended region of the Rydberg series of resonances.

region of the curve for the total recombination rate coefficients (shown later).

Fig. 2 presents photoionization cross-sections σ_{PI} of three excited levels of P II: (a) a low-lying excited level $3s 3p 3d ({}^1F_3^o)$ (top panel) and two highly excited levels (b) $3s 3p 9i ({}^3H_4^o)$ (middle panel) and (c) $3s 3p 7h ({}^1H_5)$ (bottom panel). The cross-sections of high-lying excited states start at much lower ionization thresholds than the top one. All three levels show strong Seaton resonances (shown by arrows in the figure) for dipole transitions from the ground level of the core. These transitions are specified in Table 1. A photon at an energy matching a transition energy is absorbed by the core ion for excitation, while the outer electron remains as spectator. The state leads to resonant photoionization, often with enhanced background cross-section as the core drops back to the ground level. Seaton explained these resonances in terms of PEC (Yu & Seaton 1987; Nahar & Pradhan 1991). The resonant peak is related to the radiative decay rate of the state and the enhancement can raise the background cross-sections to orders of magnitude, as seen for these three levels. The energy positions of these resonances remain about the same in photoionization of any excited level, regardless of the ionization energy of the level. The reason is that the transition energies of the core ion remain the same. These resonances make significant contributions to recombination in high-temperature plasmas.

The illustrative cross-sections in Figs 1 and 2 are presented in the photon energy ranges that correspond to a significant display of resonant features and effect on the background by excitations of the core ion. It may be noted that the features are extended be-

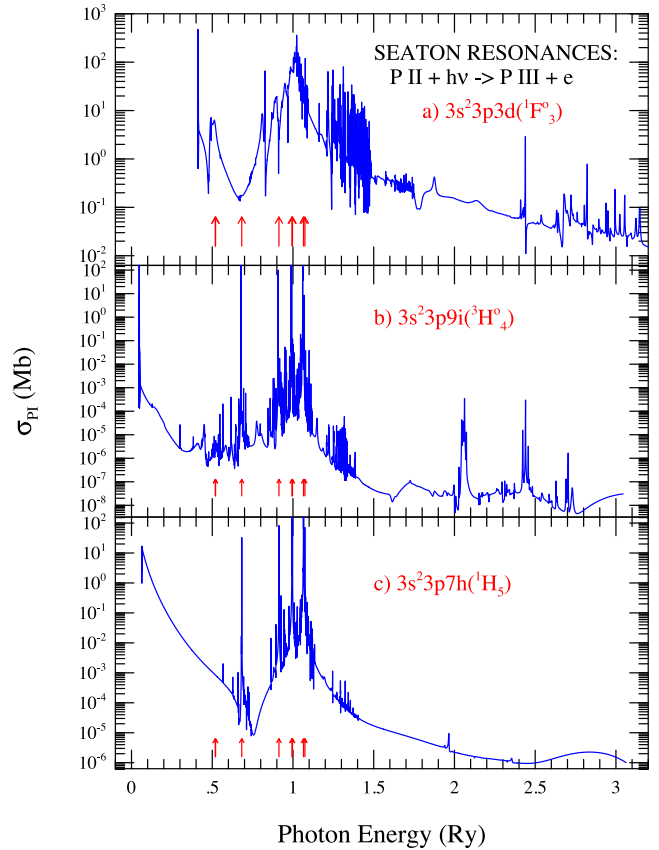


Figure 2. Photoionization cross-sections of three excited levels of P II: (a) $3s 3p 3d ({}^1F_3^o)$, (b) $3s 3p 9i ({}^3H_4^o)$ and (c) $3s 3p 7h ({}^1H_5)$, illustrating the prominent Seaton resonances (highlighted by arrows) due to PEC. Note that the positions of the resonances remain the same, regardless of the ionization threshold energies of various levels.

yond the highest core excitations included in the first term of the wavefunction in equation (3). Table 1 shows that the energy of the highest core excitation is about 1.46 Ry. If this energy is added to the ionization energy of any level in the figures, we can see that the resonant structure continues beyond the added energy, indicating contributions from higher excitations in the core. This is an effect of correlation or interaction of configurations. The present computation includes a large number of configurations for the core ion where orbitals 4d, 4f and 5s are also included and they have introduced resonances. These resonances are not as precise as the lower ones. The high-energy featureless background cross-section beyond these resonances is obtained by extrapolation, as described in the computation section. The file for photoionization cross-sections with extended energy range will be available electronically online at NORAD-Atomic-Data database (NORAD Atomic Data database <http://norad.astronomy.ohio-state.edu>).

It may be noted that P II is a near-neutral ion that exists in low-energy and low-temperature plasmas. Hence its core ion does not excite to very high-lying levels. This is the reason for choosing 18 levels in the wavefunction expansion. The dominance of core ion excitations to low-lying levels and their convergence is evident from the resonant and enhanced background features in the lower energy region and weaker resonances in the higher energy regions of photoionization cross-sections. Hence convergence of contributions for core ion excitations in the high-energy region (Nahar & Pradhan 2016) is not of much relevance.

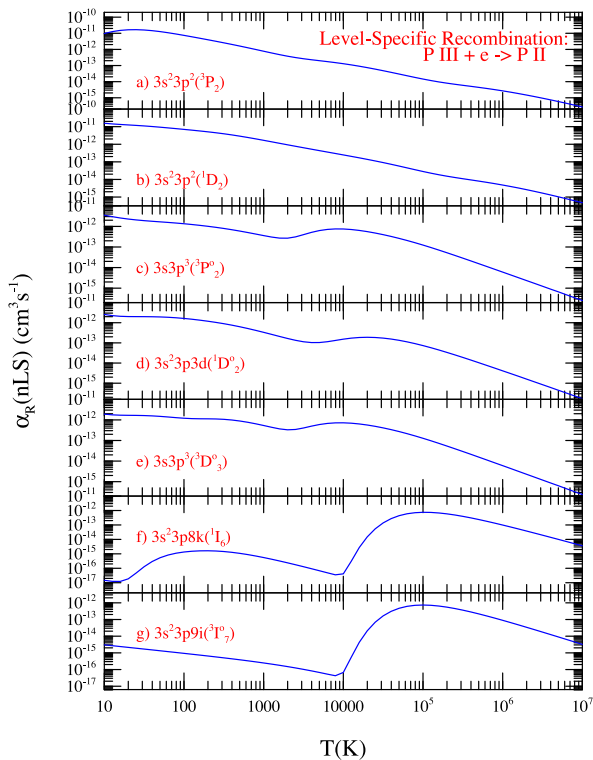


Figure 3. Maxwellian averaged level-specific recombination rate coefficients of a number of levels of P II, specified in panels (a)–(g), displaying variations with temperature. The variations depend on the energy positions and strength of resonances in photoionization cross-sections.

4.2 Electron–ion recombination

The level-specific recombination rate coefficients $\alpha_{RC}(j\pi)$ of all 475 fine-structure levels of P II with $n \leq 10$ are reported. They are often needed for the cascade matrix in models. These rates are obtained from the level-specific photoionization cross-sections as described in Section 2. Rate coefficients of each level include both RR and DR and display the shapes and structures of recombination at various temperatures.

The structures in $\alpha_{RC}(J\pi)$ of a level depend on the position and strength of the resonances as well as enhancement in the background σ_{PI} . Fig. 3 presents samples of level-specific recombination rate coefficients to illustrate such features. The top panel (a) presents $\alpha_{RC}(i)$ of the ground level, which is often a smoothly decaying curve.

Table 2. Maxwellian averaged level-specific recombination rate coefficients $\alpha_{RC}(i)$ of 10 $J\pi(n)$ levels that contribute dominantly to the total electron–ion recombination. Numbers ‘ n ’ within parentheses indicate the position of the level in the symmetry $J\pi$. BE is the binding energy of the level. The full table is available online.

log T	$J\pi$ (level)									
	$1S_0^e(2)$	$3D_1^o(1)$	$3P_2^e(1)$	$3D_2^o(2)$	$1D_2^o(4)$	$3D_3^o(1)$	$1F_3^o(4)$	$3H_4^o(30)$	$1H_5^e(13)$	$3H_6^o(11)$
BE(Ry)=	−1.26	−0.865	−1.48	−0.865	−0.732	−0.864	−0.409	−0.0443	−0.0626	−0.0494
1.0	8.56E-12	5.11E-12	9.65E-12	3.53E-12	2.58E-12	1.91E-12	3.71E-12	2.67E-16	1.48E-13	9.91E-14
1.1	7.28E-12	4.01E-12	1.27E-11	2.97E-12	2.25E-12	1.76E-12	3.07E-12	2.15E-16	1.32E-13	8.82E-14
1.2	6.29E-12	3.20E-12	1.51E-11	2.57E-12	2.08E-12	1.69E-12	2.64E-12	1.87E-16	1.18E-13	7.86E-14
1.3	5.52E-12	2.61E-12	1.65E-11	2.28E-12	2.02E-12	1.67E-12	2.37E-12	1.74E-16	1.05E-13	7.00E-14
1.4	4.89E-12	2.17E-12	1.68E-11	2.07E-12	2.01E-12	1.66E-12	2.19E-12	1.71E-16	9.33E-14	6.23E-14
1.5	4.35E-12	1.84E-12	1.60E-11	1.90E-12	2.00E-12	1.62E-12	2.06E-12	1.71E-16	8.31E-14	5.54E-14
1.6	3.87E-12	1.57E-12	1.45E-11	1.78E-12	1.98E-12	1.57E-12	1.93E-12	1.72E-16	7.40E-14	4.93E-14
1.7	3.45E-12	1.36E-12	1.27E-11	1.67E-12	1.94E-12	1.49E-12	1.79E-12	1.73E-16	6.58E-14	4.39E-14
1.8	3.07E-12	1.18E-12	1.08E-11	1.56E-12	1.86E-12	1.39E-12	1.65E-12	1.84E-16	5.85E-14	3.90E-14
1.9	2.74E-12	1.03E-12	9.02E-12	1.46E-12	1.76E-12	1.29E-12	1.49E-12	2.22E-16	5.20E-14	3.46E-14

However, the existence of a resonance at the threshold and a broad resonance near it has introduced a curvature at very low temperature. The ground and $3s^2 3p^2 (^1D_2)$ levels of the ground configuration in panels (a) and (b) show a relatively smooth and featureless rate coefficient compared with the other excited levels presented in the figure. Levels (c) $3s 3p^3 (^3P_2^o)$, (d) $3s^2 3p 3d (^1D_2^o)$, (e) $3s 3p^3 (^3D_3^o)$ and (g) $3s^2 3p 9i (^3I_7^o)$ have high recombination, with some variations at low temperature and a prominent ‘DR’ bump at high temperature. However, level (f) $3s^2 3p 8k (^1I_6)$ starts with almost no recombination, because its σ_{PI} has no resonance and low background in the low-energy region. However, the presence of a large DR bump shows that it dominates recombination at high temperature.

The recombination rate coefficients of the 475 levels were processed for dominance at various low and high temperatures. A level does not typically remain dominant for the entire temperature range, due to variations in the structure of its $\alpha_{RC}(J\pi)$. At each temperature, the set of levels that contribute to 80 per cent of the total α_{RC} was obtained. Table 2 presents $\alpha_{RC}(j\pi)$ of a number of levels that make the dominant contributions to the total rate coefficient at 10 different temperatures. The complete table of energies with spectroscopic identification and $\alpha_{RC}(j\pi)$ of all levels will be available electronically at NORAD-Atomic-Data.database (NORAD Atomic Data database <http://norad.astronomy.ohio-state.edu>).

The total recombination rate coefficients $\alpha_{RC}(T)$ are obtained for the entire temperature range by summing the contributions of level-specific rate coefficients of all 475 levels and those from high- n levels as described by the unified method. Typically, the rate coefficient decreases smoothly in the low-temperature region. However, for P II a slight curvature in $\alpha_{RC}(T)$ is visible in the very low temperature region around 330 K (Fig. 4). This is the effect of the existence of threshold and low-energy resonances in photoionization of many P II levels, as illustrated above. With 14 electrons, the ion has strong electron–electron interaction, which causes considerable interference between RR and DR as seen in other low charge ions, such as for P II (Nahar 1997). The effect is seen prominently in the shape of $\alpha_{RC}(T)$ around a temperature of 6700 K in Fig. 4. It is the region of interference where the unified method provides the most precise total recombination rate coefficient, while the summed total from individually calculated RR and DR rate coefficients is the most uncertain. With an increase of temperature, DR becomes more prominent from resonances formed with excitations of the core ion and this results in a DR bump around temperature 10^5 K. Beyond this temperature, α_{RC} decays monotonically. However, inclusion of higher excitations of the core could introduce more resonances in photoionization, which would raise α_{RC} somewhat in the

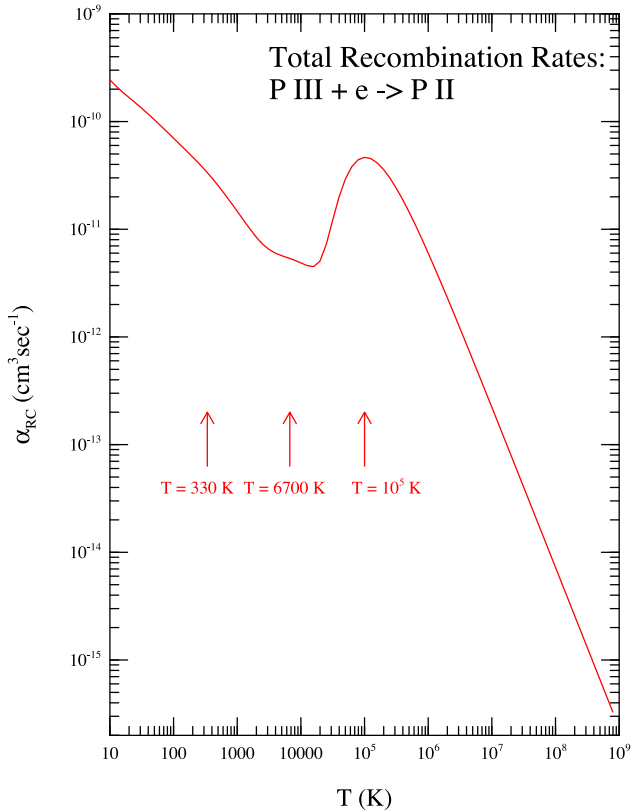


Figure 4. Total recombination rate coefficient α_{RC} ($\text{cm}^3 \text{s}^{-1}$) with respect to temperature. The features include a slight curvature at a very low temperature of about 330 K, a strong interference effect of RR and DR in the temperature region around 6700 K and a high-temperature bump due to the dominance of DR at 10^5 K.

high-temperature region. The present work considers excitations of 17 levels of the core ion P III, assuming low probability for higher excitations in the high-temperature region, where this near-neutral ion may not exist. However, modelling often requires values of α_{RC} over a very large temperature range. From the energy range of the resonant complexes, the accuracy of α_{RC} is expected to be high within 15 per cent over a million degrees. The values of $\alpha_{RC}(T)$ in ($\text{cm}^3 \text{s}^{-1}$) are tabulated in Table 3.

A Maxwellian averaged $\alpha_{RC}(T)$ gives smooth variations with temperature. However, the detailed spectrum of the summed total recombination cross-section σ_{RC} and rate coefficient $\alpha_{RC}(E)$ with photoelectron energy E shows resonant features that match those of photoionization cross-sections. These recombination lines could be seen in the astrophysical spectra as satellite lines and are identifiable for a few electron systems. Fig. 5 presents the resonant recombination spectrum of P II, $\sigma_{RC}(E)$ in the top panel and $\alpha_{RC}(E)$ in the bottom panel, with respect to photoelectron energy. $\alpha_{RC}(E)$ can be measured in a laboratory where energies are expressed in eV. The arrows in the figure indicate various excitation thresholds of the core where the resonances converge. It may be noted that $\alpha_{RC}(E)$ drops off after the excitation energies. This is due to the release of trapped electrons in DR after the excitation energies.

4.3 Conclusion

The inverse processes of photoionization and electron–ion recombination of P II have been studied using the unified method. The highlighted findings are as follows.

Table 3. Total recombination rate coefficients of P II. The full table is available online.

$\log_{10}(T)$ (K)	α_{RC} ($\text{cm}^3 \text{s}^{-1}$)	$\log_{10}(T)$ (K)	α_{RC} ($\text{cm}^3 \text{s}^{-1}$)
1.0	2.4383E-10	5.1	4.5244E-11
1.1	2.1225E-10	5.2	4.1280E-11
1.2	1.8748E-10	5.3	3.5784E-11
1.3	1.6707E-10	5.4	2.9768E-11
1.4	1.4913E-10	5.5	2.3967E-11
1.5	1.3273E-10	5.6	1.8801E-11
1.6	1.1762E-10	5.7	1.4444E-11
1.7	1.0378E-10	5.8	1.0915E-11
1.8	9.1144E-11	5.9	8.1413E-12
1.9	7.9985E-11	6.0	6.0093E-12
2.0	6.9989E-11	6.1	4.3988E-12
2.1	6.1260E-11	6.2	3.1989E-12
2.2	5.3616E-11	6.3	2.3150E-12
2.3	4.6842E-11	6.4	1.6672E-12
2.4	4.0741E-11	6.5	1.1974E-12
2.5	3.5157E-11	6.6	8.5753E-13
2.6	3.0047E-11	6.7	6.1292E-13
2.7	2.5420E-11	6.8	4.3755E-13
2.8	2.1290E-11	6.9	3.1169E-13
2.9	1.7732E-11	7.0	2.2197E-13
3.0	1.4675E-11	7.1	1.5789E-13
3.1	1.2126E-11	7.2	1.1222E-13
3.2	1.0051E-11	7.3	7.9738E-14
3.3	8.4332E-12	7.4	5.6640E-14
3.4	7.2590E-12	7.5	4.0224E-14
3.5	6.4776E-12	7.6	2.8549E-14
3.6	5.9927E-12	7.7	2.0257E-14
3.7	5.6786E-12	7.8	1.4407E-14
3.8	5.4207E-12	7.9	1.0200E-14
3.9	5.1589E-12	8.0	7.2392E-15
4.0	4.8675E-12	8.1	5.1342E-15
4.1	4.5929E-12	8.2	3.6411E-15
4.2	4.4968E-12	8.3	2.5826E-15
4.3	5.0664E-12	8.4	1.8318E-15
4.4	7.2738E-12	8.5	1.2995E-15
4.5	1.2180E-11	8.6	9.2157E-16
4.6	1.9974E-11	8.7	6.5381E-16
4.7	2.9378E-11	8.8	4.6361E-16
4.8	3.8141E-11	8.9	3.2896E-16
4.9	4.4196E-11	9.0	2.3350E-16
5.0	4.6516E-11		

(i) Although P II is a low charged ion, relativistic effects are found to be important in very low-energy photoionization. A threshold resonance appears in photoionization of the ground and many excited levels formed by the couplings of fine-structure channels. These and a broad resonant structure near the threshold in levels of the ground state have produced a slight curvature in the total $\alpha_{RC}(T)$ curve in the very low temperature region around 330 K. Relativistic effects are not important in the higher energy region for near-neutral ions (e.g. C II: Nahar 2002).

Radiation damping is included in the present results but found not to be significant. For core ion excitations to high-lying levels of highly charged ions, the Auger effect broadens the resonances near the excitation threshold; this was studied along with radiation damping by Robicheaux et al. (1995).

(ii) Extensive resonances in low-energy photoionization, due to electron–electron correlation effects, show an impact on the curves of level-specific recombination rates and considerable interference

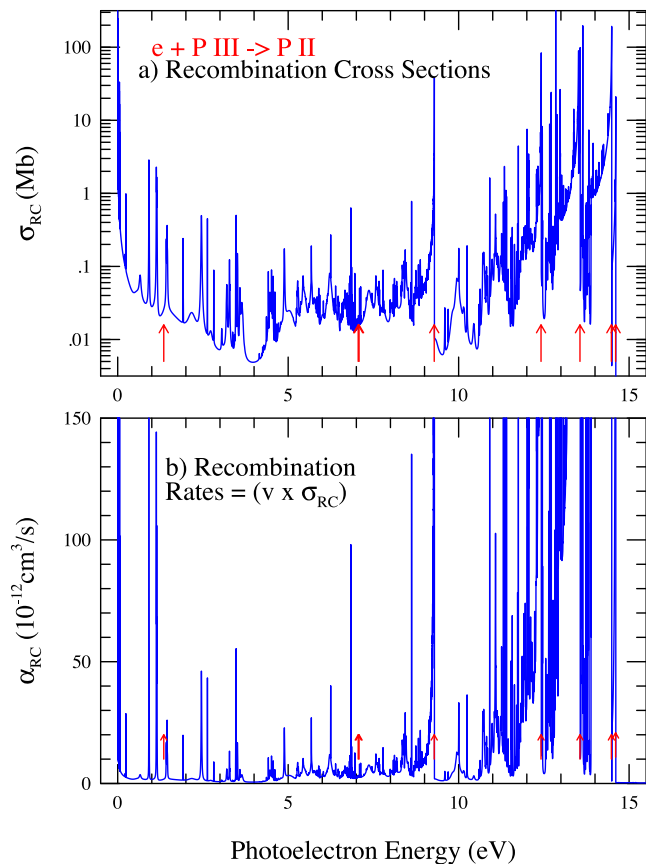


Figure 5. Recombination spectrum of P II: (a) total recombination cross-section σ_{RC} (Mb) and (b) total recombination rate coefficient $\alpha_{RC}(E)$ with respect to photoelectron energy. The arrows indicate various excitation thresholds of the core where the resonances converge.

of RR and DR in the low-temperature region around 6700 K of the total rate coefficient.

(iii) Dominating high-peak Seaton resonances due to photo-excitation of the core are found in the high-energy region. They enhance the background photoionization cross-section by the order of magnitude of many excited levels and make an important contribution to high-temperature recombination rates. The total recombination rate has a high peak at a temperature of 10^5 K.

(iv) Detailed recombination cross-sections $\sigma_{RC}(E)$ and recombination rate coefficients $\alpha_{RC}(E)$ with respect to photoelectron energies are presented for possible observations and measurements.

(v) Based on the accuracy of the results obtained and the unified method, the present results are expected to have an accuracy of 15–30 per cent for over 1 MK and are applicable to many astrophysical applications.

All the atomic data for photoionization cross-sections and rates of electron–ion recombination, including Tables 2 and 3, will be available online from NORAD Atomic Data at <http://norad.astronomy.ohio-state.edu>.

ACKNOWLEDGEMENTS

This work was partially supported by a grant from the NSF programme AST–1312441. The computational work was carried out at the Ohio Supercomputer Center in Columbus Ohio.

REFERENCES

- Bell R. H., Seaton M. J., 1985, *J. Phys. B*, 18, 1589
- Berrington K. A., Eissner W., Norrington P. H., 1995, *Comput. Phys. Commun.*, 92, 290
- Burke P. G., Taylor K. T., 1975, *J. Phys. B*, 8, 2620
- Eissner W., Jones M., Nussbaumer N., 1974, *Comput. Phys. Commun.*, 8, 270
- Hinojosa G. et al. 2015, Photoionization Cross Sections of P ii: Theory & Measurement. 46th Annual Meeting of the APS Division of Atomic, Molecular and Optical Physics (DAMOP), Vol 60 No 7: Abstract: T5.00008 No 7, June 8–12; Columbus, Ohio, American Physical Society, USA
- Hummer D. G., Berrington K. A., Eissner W., Pradhan A. K., Saraph H. E., Tully J. A., 1993, *A&A*, 279, 298
- Molaro P., Levshakov S. A., D’Odorico S., Bonifacio P., 2001, *ApJ*, 549, 90
- Nahar S. N., 1996, *Phys. Rev. A*, 53, 2417
- Nahar S. N., 1997, *Phys. Rev. A*, 55, 1980
- Nahar S. N., 2002, *Phys. Rev. A*, 65, 052702
- Nahar S. N., 2017, *New Astron.*, 50, 19
- Nahar S. N., Pradhan A. K., 1991, *Phys. Rev. A*, 44, 2935
- Nahar S. N., Pradhan A. K., 1992, *Phys. Rev. Lett.*, 68, 1488
- Nahar S. N., Pradhan A. K., 1994, *Phys. Rev. A*, 49, 1816
- Nahar S. N., Pradhan A. K., 2006, *Phys. Rev. A*, 73, 062718
- Nahar S. N., Pradhan A. K., 2016, *Phys. Rev. Lett.*, 116, 235003
- Nahar S. N., Pradhan A. K., Zhang H., 2000, *ApJS*, 131, 375
- Nahar S. N., Eissner W., Chen G.-X., Pradhan A. K., 2003, *Astron. Astrophys.*, 487, 789
- Nahar S. N. et al., 2017, *J. Quant. Spectr. Radiative Transfer*, 187, 215
- National Institute of Standards and Technology (NIST) Gaithersburg MD, Kramida A., Ralchenko Yu., Reader J., NIST ASD Team, 2015, NIST Atomic Spectra Database (ver.5.3), http://physics.nist.gov/PhysRefData/ASD/levels_form.html
- Opacity Project Team, 1995, *The Opacity Project Vol. 1*. Institute of Physics Publishing, England
- Opacity Project Team, 1996, *The Opacity Project Vol. 2*. Institute of Physics Publishing
- Pradhan A. K., Zhang H. L., 1997, *J. Phys. B*, 30, L571
- Pradhan A. K., Nahar S. N., 2011, *Atomic Astrophysics and Spectroscopy*. Cambridge Univ. Press, Cambridge
- Pradhan A. K., Nahar S. N., Zhang H., 2001, *ApJ*, 549, L265
- Robicheaux F., Gorczyca T. W., Griffin D. C., Pindzola M. S., Badnell N. R., 1995, *Phys. Rev. A*, 52, 1319
- Sakimoto K., Terao M., Berrington K. A., 1990, *Phys. Rev. A*, 42, 291
- Scott N. S., Burke P. G., 1980, *J. Phys. B*, 12, 4299
- Seaton M. J., 1987, *J. Phys. B*, 20, 6363
- Welsh B. Y., Sfeir D. M., Sallmen S., Lallemand R., 2001, *A&A*, 372, 516
- Yu Y., Seaton M. J., 1987, *J. Phys. B*, 20, 6409
- Zhang H. L., Nahar S. N., Pradhan A. K., 1999, *J. Phys. B*, 32, 1459

SUPPORTING INFORMATION

Supplementary data are available at [MNRAS](https://www.mnras.org) online.

Table 2. Maxwellian averaged level-specific recombination rate coefficients $\alpha_{RC}(i)$ of $10 J\pi(n)$ levels that contribute dominantly to the total electron–ion recombination.

Table 3. Total recombination rate coefficients of P II.

Please note: Oxford University Press is not responsible for the content or functionality of any supporting materials supplied by the authors. Any queries (other than missing material) should be directed to the corresponding author for the article.